J. Fluid Mech. (1995), *vol.* 293, *pp.* 1–23

On vapour flow in a hot porous layer

By SHAUN D. FITZGERALD† AND ANDREW W. WOODS

Institute of Theoretical Geophysics, Department of Applied Mathematics and Theoretical Physics and Department of Earth Sciences, University of Cambridge CB3 9EW, UK

(Received 18 November 1993 and in revised form 9 January 1995)

The motion of isothermal vapour in a permeable rock is governed by a nonlinear diffusion equation for the vapour pressure. We analyse vapour flow described by this equation in both bounded and unbounded domains. We then apply these solutions to describe the controls on the rate of vaporization of liquid invading a hot permeable rock. In an unbounded domain, we determine asymptotic similarity solutions describing the motion of vapour when it is either supplied to or removed from the reservoir. Owing to the compressibility, these solutions have the property that vapour surfaces migrate towards the isobar on which the vapour has the maximum speed.

In contrast, if vapour is supplied to or removed from a closed bounded system sufficiently slowly then the vapour density and pressure rapidly become approximately uniform. As more vapour is added, the mean pressure gradually increases and vapour surfaces become compressed. If liquid slowly invades a hot bounded porous layer and vaporizes, the vapour pressure becomes nearly uniform. As more liquid is added, the reservoir gradually becomes vapour saturated and the vaporization ceases.

In an open bounded system, with a constant rate of vapour injection, the flux of vapour across the reservoir becomes uniform. If liquid is injected slowly and vaporizes then again the vapour flux becomes spatially uniform. However, the vapour flux now increases slowly as the liquid invades further into the rock, as a result of the decreased resistance to vapour flow from the interface to the far boundary.

1. Introduction

Geothermal power is generated from the vast reserves of thermal energy in the Earth's crust by withdrawing hot fluids from geothermal reservoirs. These fluids are then passed through turbines to produce electricity or heat exchangers for domestic heating. The most effective geothermal power systems, such as in the Geysers, California and Larderello, Italy, draw vapour from vapour-saturated layers of hot fractured rock and permeable sediment, and extract the thermal energy by passing this vapour through turbines.

Vapour-dominated geothermal reservoirs are naturally recharged as meteoric water percolates into the reservoir, is heated and vaporizes (Truesdell & White 1973). However, owing to the high rates of extraction of vapour for power generation, there has been a significant reduction in the fluid levels and pressures of certain geothermal reservoirs (Kerr 1991; Enedy 1989). This has reduced their ability to generate geothermal power and so many commercial operators have initiated active water injection programmes in an attempt to build up the reservoir pressures. As a consequence, there has been much interest in the nature of the fluid flows within such reservoirs (Pruess *et al.* 1987; Woods & Fitzgerald 1993).

† Present address: Department of Petroleum Engineering, Stanford University, Stanford, CA 94305, USA.

Hydrothermal systems are commonly thought to exist in a dynamic state in which fluid circulates within fractured porous rock (Cathles 1977; Donaldson 1962; Dunn & Hardee 1981; Hurst & Dibble 1981; Parmentier & Schedl 1981; Grant, Donaldson & Bixley 1982; Wohletz & Heiken 1992). In developing a model of such flows, one must characterize the microscopic flows through the fractures and pores in order to describe the macroscopic flows on the scale of a reservoir. The relative resistance to flow through fractures and pores is dependent upon the fracture apertures and spacing and the permeability of the porous matrix. Effects of the fractures upon the fluid flow within geothermal reservoirs are often inferred from detailed measurements of pressure and temperature within wells used for the extraction or injection of fluid (Fradkin, Sorey & McNabb 1981; Goyal & Box 1990; Axelsson & Bodvarsson 1987). In many reservoirs, such as Kawah Kamojang in Indonesia (Wohletz & Heiken 1992), The Geysers in California, Larderello in Italy, Ahuachapan in El Salvador and Kawerau in New Zealand (Grant *et al.* 1982), the majority of the fluid flows are believed to occur within the fractures. However, in other reservoirs, such as the East Mesa reservoir, California, the flows occur primarily within a porous matrix (Grant *et al.* 1982). In this work, we adopt a porous flow model to describe the transport of liquid and vapour. This model is particularly appropriate for this latter type of reservoir. However, the model also provides insight into the flows within highly fractured reservoirs.

Using a porous matrix model, the volume flux per unit area $\boldsymbol{u}$ may be related to the interstitial velocity $\boldsymbol{v}$ by

$$\boldsymbol{u} = \phi \boldsymbol{v}, \tag{1}$$

where ϕ is the void fraction (Bear 1972; Phillips 1991). In many geothermal reservoirs the fluid velocities $\boldsymbol{u}$ through a geothermal reservoir are very low so that viscous frictional forces are much greater than the inertial forces, and the interstitial Reynolds number, $R = \rho v d/\mu$ is small, $R \ll 1$ (Rubin & Schweitzer 1972). Here ρ represents the density of the fluid which has values $\sim 10^3$ and ~ 10 kg m^{-3} for liquid and vapour, μ the dynamic viscosity which is $\sim 10^{-4}$ and $\sim 10^{-5}$ kg ms^{-1} for liquid and vapour, d a typical pore size $\sim 10^{-4}$ m, and v the interstitial speed. The condition $R \ll 1$ is satisfied for liquid and vapour flows for interstitial speeds of $v < 10^{-4}$ and $v < 10^{-3}$ m s^{-1} respectively. Previous studies of natural fluid circulation in geothermal reservoirs have shown that liquid velocities are typically less than 10^{-6} m s^{-1} (Donaldson 1962, 1968; Norton & Knight 1977; Cline, Bodnar & Rimstidt 1992) and so the flows are of low Reynolds number. In the case of low Reynolds number, the volume flux per unit area $\boldsymbol{u}$ is given by Darcy's law

$$\mu \boldsymbol{u} = -k(\nabla P - \rho \boldsymbol{g}), \tag{2}$$

where ∇P is the applied pressure gradient, $\boldsymbol{g}$ is the gravitational acceleration and k is the permeability (Bear 1972; Rubin & Schweitzer 1972; Dullien 1992).

If the fluid speed v and the typical grain size D are sufficiently small then the timescale for fluid and solid to thermally equilibrate, D^2/κ, is much shorter than the timescale for the advection of heat across a grain, D/v, and the medium becomes locally isothermal. Thus for a typical grain size of 0.5 mm, the condition for local thermal equilibrium is the same as that for low-Reynolds-number flows, $v \leqslant 10^{-3}$ m s^{-1} since typically the thermal diffusivity of rock $\kappa \sim 2 \times 10^{-6}$ m^2 s^{-1}.

For simplicity, geothermal reservoirs are often modelled as being isotropic (Dullien 1992; Phillips 1991). This approximation is appropriate if in addition to the limits on fluid velocity mentioned above, there is no large-scale alignment of fractures to provide preferred flow directions. Although a simplification, such models provide useful insight into many of the underlying processes.

In the following analysis we assume that the rock may be modelled as an isotropic porous medium in which Darcy's law (2) is valid and in which the rock and fluid are in local thermal equilibrium. Although a simplification of the real situation, the model provides a framework in which many of the underlying controls on the macroscopic fluid flows within geothermal reservoirs may be understood. The general principles can then be applied to interpret results of more complex models of the microscopic flow.

Using such a model for the microscopic flow, in a previous paper (Woods & Fitzgerald 1993) we analysed the controls on the rate of vaporization of a liquid front injected into an unbounded hot vapour-saturated permeable rock. We presented similarity solutions to describe the rate of vapour generation if the liquid front advances at a rate proportional to $t^{1/2}$. These solutions identified that as the flow rate increases, the fraction of liquid which vaporizes decreases. This is because at higher flow rates, the interfacial pressure required to drive new vapour ahead of the front increases. Therefore, in equilibrium, the interfacial temperature increases, reducing the heat released from the rock for vaporization. In the present paper, we build upon this work by examining the motion of isothermal vapour in one dimension in both bounded and unbounded domains. We use these results to investigate the different controls that the vapour motion can have on the rate of vaporization in a bounded domain.

First, we describe the motion of vapour injected into a permeable rock, and distinguish between the self-similar flows which develop in an unbounded domain and vapour flow in a bounded region. We also identify the difference between the motion of vapour and pressure surfaces which migrate at quite different rates owing to the compressibility of the vapour. This is of importance when chemical or radioactive tracers are injected into geothermal reservoirs, since we show that changes in the pressure and flow rate may occur some time before any change in the fluid chemistry may be detected (D'Amore *et al.* 1977; Duchi, Minissale & Manganelli 1992; Martini *et al.* 1991). Next we show that when vapour is injected into a bounded domain sufficiently slowly, the vapour pressure becomes nearly uniform. We use this result to develop a spatially averaged model of the rate of vaporization of a liquid front migrating into a bounded hot porous layer, and successfully compare this with a full numerical model. Finally, we consider the simultaneous injection and extraction of vapour from a bounded porous rock. We show that once vapour has migrated across the reservoir, the mass flux through the reservoir becomes nearly uniform. Using this result, we develop a quasi-steady model to describe the vaporization of a liquid front slowly invading an open reservoir. By comparison with a full numerical model, we show that this quasi-steady model is very accurate for times greater than the time for the dynamic pressure signal to migrate across the reservoir. We conclude with a discussion of the relevance of our work to geothermal systems including estimates of the timescale for pressure build-up and for the migration of a liquid front through a model geothermal reservoir.

2. Unbounded vapour flow

In most cases of interest the pressure gradients ∇P within the vapour are significantly greater than the gravitational force $\rho \boldsymbol{g}$ and so the vapour moves with velocity $\boldsymbol{u}$ given by a simplified version of Darcy's law (2)

$$\boldsymbol{u} = -\frac{k}{\mu}\nabla P, \tag{3}$$

where, as before, k represents the permeability of the medium, μ the dynamic viscosity of the vapour and P the pressure. Owing to the thermal inertia of porous layers (Bodvarsson 1972), the vapour remains approximately isothermal and the pressure is linearly related to the density ρ according to the equation of state

$$P = \rho R_g T \tag{4}$$

where R_g is the gas constant and T is the absolute temperature. Combining (3) and (4) with the conservation of mass

$$\phi \frac{\partial \rho}{\partial t} + \nabla \cdot (\rho \boldsymbol{u}) = 0 \tag{5}$$

one may derive the equation governing the pressure distribution associated with the migration of vapour (Elder 1981):

$$\frac{\partial P}{\partial t} - \frac{k}{\phi \mu} \nabla \cdot (P \nabla P) = 0, \tag{6}$$

where the medium has porosity ϕ. In an unbounded reservoir, under certain conditions, the vapour motion may be described in terms of self-similar solutions. These provide useful insight into some features of vapour motion.

In the main text, we restrict attention to one-dimensional flow solutions, as these reveal many of the important features of the flow. However, for completeness, in an Appendix, we describe vapour motion in other geometries.

2.1. *Injection or extraction at constant pressure*

For injection or extraction with constant pressure maintained at the source or sink, it is useful to introduce the dimensionless pressure $p = (P - P_\infty)/(P_{max} - P_{min})$. This is defined in terms of the maximum and minimum vapour pressures, P_{max} and P_{min}, which depend directly upon the imposed boundary conditions, and P_∞, the far-field pressure. In the case of injection, P_{max} is the pressure at the source and $P_{min} = P_\infty$ whereas in the case of extraction, $P_{max} = P_\infty$ and P_{min} is the pressure at the sink. Equation (6) may then be expressed as

$$\frac{\partial p}{\partial t} - \alpha \frac{\partial}{\partial x}\left[(p + p_\infty)\frac{\partial p}{\partial x}\right] = 0, \tag{7}$$

where $p_\infty = P_\infty/(P_{max} - P_{min}) > 0$ and the diffusion coefficient $\alpha = k(P_{max} - P_{min})/\phi\mu$. To describe the injection of vapour at a constant pressure we set $p = 1$ at $x = 0$, and $p \to 0$ as $x \to \infty$. Now (7) admits exact similarity solutions, $p = p(\eta)$, with similarity variable $\eta = x/2(\alpha t)^{1/2}$, where p satisfies

$$(p_\infty + p)p'' + (p')^2 + 2\eta p' = 0 \tag{8}$$

and the boundary conditions $p(0) = 1$ and $p(\infty) = 0$. In figure 1 we show numerical solutions for the self-similar vapour pressure p as a function of $\eta/p_\infty^{1/2}$, for several values of the background pressure p_∞. As p_∞ increases, the effective diffusion coefficient $(p_\infty + p)$ associated with the vapour motion becomes approximately constant and the self-similar pressure distribution tends to $p = \operatorname{erfc}(\eta/p_\infty^{1/2})$ (dashed line). These solutions correspond to the injection of vapour into the reservoir at a rate $Q(t/t^*)^{-1/2}$, where the flux

$$Q = -p'(0)\, P_\infty \phi/(RT)^{1/2} \tag{9}$$

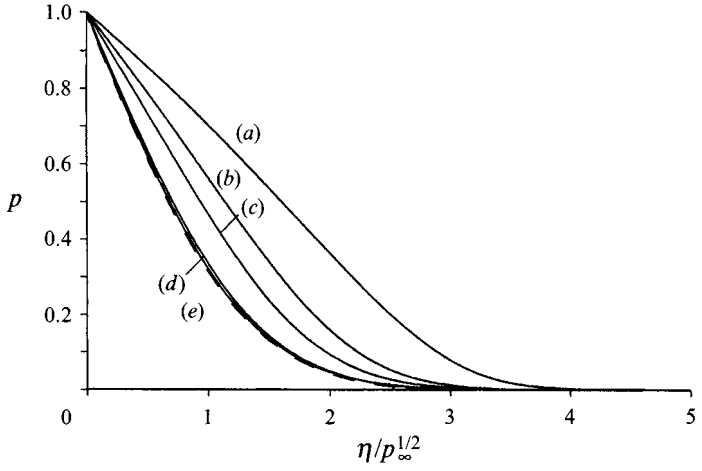

FIGURE 1. The dimensionless pressure in the rock as a function of $\eta/p_\infty^{1/2}$ as vapour is injected at a constant pressure. The dashed line shows the distribution of pressure for the case in which $p_\infty \to \infty$. The solid lines show the cases for (*a*) $p_\infty = 0.2$, (*b*) $p_\infty = 0.5$, (*c*) $p_\infty = 1$, (*d*) $p_\infty = 10$ and (*e*) $p_\infty = 100$.

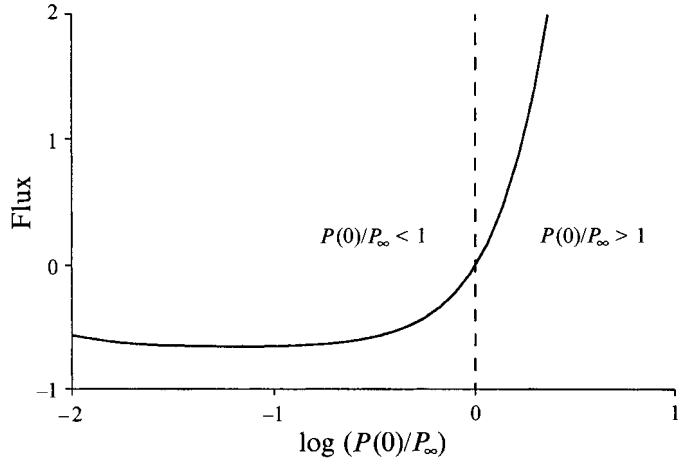

FIGURE 2. Variation of the vapour flux with $P(0)/P_\infty$.

and the timescale

$$t^* = kP_\infty/\phi R_g T\mu. \tag{10}$$

In figure 2 we show that the flux PP'/P_∞^2 increases with the injection pressure (the case $P(0)/P_\infty > 1$).

To describe the extraction of vapour at a constant pressure, we set $p = -1$ at $\eta = 0$ and $p \to 0$ as $\eta \to \infty$. We also restrict attention to situations in which the total pressure remains positive, $p_\infty > 1$. In figure 3 we show the self-similar distribution of vapour as a function of $\eta/p_\infty^{1/2}$ as vapour is extracted at a constant pressure from the position $\eta = 0$. As the magnitude of the background pressure, p_∞, increases, the vapour pressure distribution approaches the error function $p = \mathrm{erf}(\eta/p_\infty^{1/2})$ (dashed line). We also show in figure 2 the extracted flux, PP'/P_∞^2, as a function of the extraction pressure (the case $P(0)/P_\infty < 1$).

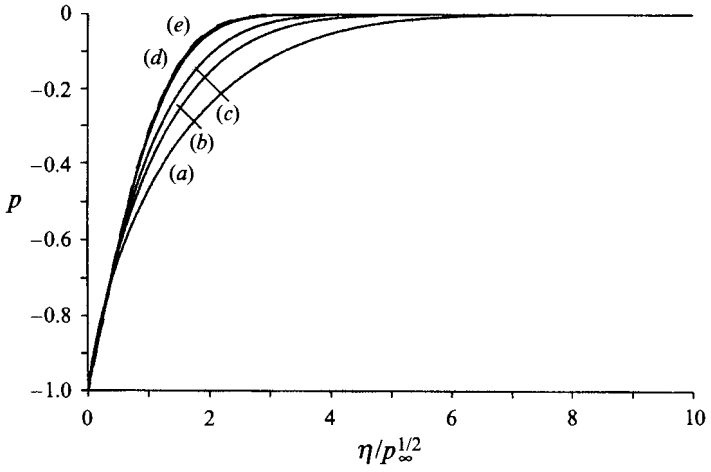

FIGURE 3. The dimensionless pressure in the rock as a function of $\eta/p_\infty^{1/2}$ as vapour is extracted at a constant pressure of $p = 0$. The dashed line shows the distribution of pressure for the case in which $p_\infty \to \infty$. The solid lines show the cases for (*a*) $p_\infty = 1.2$, (*b*) $p_\infty = 1.5$, (*c*) $p_\infty = 2$, (*d*) $p_\infty = 11$ and (*e*) $p_\infty = 101$.

These solutions illustrate the asymmetry between injection and extraction of vapour. During vapour extraction, the pressure gradient and vapour speed decrease monotonically with η. During vapour injection, the pressure gradient has a minimum some distance ahead of the source, at $2\eta = -p'$, and this corresponds to the point of maximum vapour speed.

2.2. *Motion of vapour surfaces and passive tracers*

The self-similar solutions reveal the difference between the motion of isobars and actual vapour surfaces. The vapour originally in place in the reservoir must be displaced through compression before new vapour can invade the reservoir. By identifying the regions of space in which the vapour is compressed and in which the vapour can expand, we can identify the front of the new vapour as it invades the reservoir.

According to the similarity solution, the position of the isobar $p(\eta)$ is given by

$$x_i = 2\eta(\alpha t)^{1/2}, \tag{11}$$

and has speed

$$\mathrm{d}x_i/\mathrm{d}t = \eta(\alpha/t)^{1/2}. \tag{12}$$

The speed of the vapour is given by

$$\frac{\mathrm{d}x_p}{\mathrm{d}t} = -\frac{1}{2}\frac{\mathrm{d}p}{\mathrm{d}\eta}\left(\frac{\alpha}{t}\right)^{1/2}. \tag{13}$$

Therefore, at any fixed value of η, the relative speed of vapour and isobars is a constant multiple of the isobar speed. Near the source at $\eta = 0$, $p' < 0$ and $p'' < 0$. Therefore $\mathrm{d}x_p/\mathrm{d}t > \mathrm{d}x_i/\mathrm{d}t$ and the vapour migrates relative to the isobars into regions of lower pressure. This corresponds to the decompression of the input vapour as it invades the reservoir. The similarity solution (figure 1) also shows that as $\eta \to \infty$, $p' \to 0$ and so far from the source the isobars move more rapidly than the vapour, $\mathrm{d}x_i/\mathrm{d}t > \mathrm{d}x_p/\mathrm{d}t$. This corresponds to the compression of the vapour originally in place in the reservoir. There

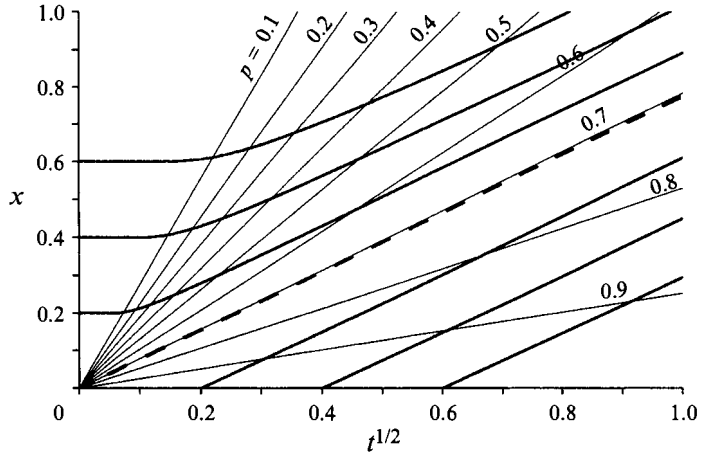

FIGURE 4. The positions of tracer particles (thick solid lines) and isobars (thin solid lines) as a function of time as vapour is injected at a constant pressure into an unbounded volume of vapour-filled hot porous rock from a planar source. The position of the front of new vapour (dashed line) is shown for the case in which $p_\infty = 1$.

is a point, $\eta = \eta^*$ say, at which the isobars and the vapour move with the same speed. This point corresponds to the leading edge of the new vapour as it advances into the reservoir. It follows from (12) and (13) that at this point, $\eta^* = -\frac{1}{2}p'(\eta^*)$. In order that the vapour converges to the isobar $p(\eta^*)$, the vapour must have the maximum velocity at $\eta = \eta^*$; that this is the case may be seen from (8), since p' attains its minimum at $\eta = \eta^*$.

For illustration, in figure 4 we show how the positions of vapour surfaces (thick solid lines) and isobars (thin solid lines) vary as a function of time as vapour is injected into the rock at a constant pressure. The position of the front of new vapour, which corresponds to the position of the isobar $p(\eta^*)$ is shown by the dashed line. The newly input vapour, in the region $\eta < \eta^*$, decompresses and so vapour surfaces migrate into regions of lower pressure. The original vapour, in the region $\eta > \eta^*$, is compressed. As a result, changes in reservoir pressure occur before new vapour reaches any particular point.

The pressure at the front of the input vapour varies as a function of the far-field pressure, p_∞ (figure 5). In general, if the background pressure is low, $p_\infty \ll 1$, there is relatively little original vapour in the reservoir and so the pressure at the front of new vapour is similar to the background value, $p \sim 0$. In contrast, if the amount of vapour initially in place is large, $p_\infty \gg 1$, then much of the pressure difference between the injection point and the far field is used to compress the original vapour. Consequently, the dimensionless pressure of the leading edge of new vapour is relatively high and at any point in the reservoir the time delay between changes in pressure and the arrival of new vapour is large. For the example shown in figure 4, $p_\infty = 1$, and at the front of new vapour $p \sim 0.7$.

2.3. *Asymptotic similarity solutions for injection*

In the limit of negligible background pressure, $P \gg P_\infty$, equation (7) has the asymptotic form

$$\frac{\partial P}{\partial t} = \frac{k}{\phi\mu}\frac{\partial}{\partial x}\left[P\frac{\partial P}{\partial x}\right]. \tag{14}$$

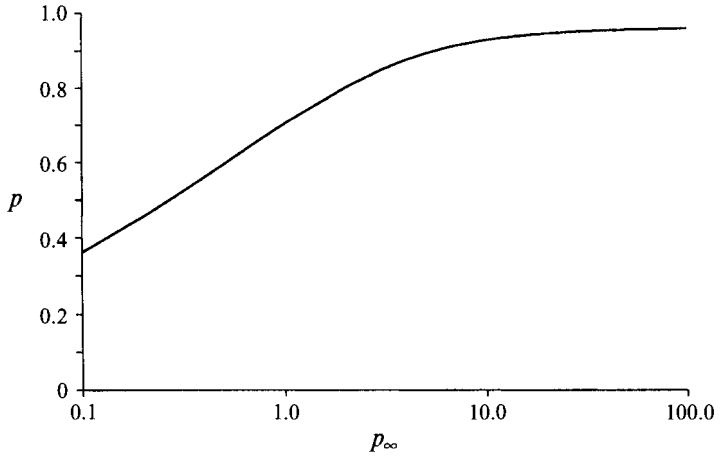

FIGURE 5. Pressure at the leading edge of the new vapour $\eta = \eta^*$ as a function of the reservoir pressure p_∞.

In this case, there is a much wider class of asymptotic similarity solutions of the form

$$p = \left(\frac{t}{t^*}\right)^{\omega} f\left(\frac{x}{L}\left(\frac{t}{t^*}\right)^{\beta}\right) \tag{15}$$

which describe the injection of vapour at a rate $Q(t/t^*)^{\gamma}$. Here the pressure scale P_o is given by

$$P_o = Q(R_g T)^{1/2}/\phi. \tag{16}$$

For convenience we have chosen the length- and timescales, L and t^*, as those corresponding to vapour flow with speed $(R_g T)^{1/2}$ driven by the imposed flux so that

$$L = kP_o/(\phi\mu(R_g T)^{1/2}), \tag{17}$$

$$t^* = kP_o/(R_g T\mu\phi), \tag{18}$$

with the dimensionless pressure defined as $p = P/P_o$. To satisfy (14) and the boundary condition at $x = 0$ that $-(k/\mu R_g T)\, PP_x = Q(t/t^*)^{\gamma}$, we require that $\beta = \frac{1}{3}(\gamma+2)$, $\omega = \frac{1}{3}(2\gamma+1)$ and that f is governed by the equation

$$ff'' + f'^2 = \tfrac{1}{3}(\gamma+2)\,\eta f' + \tfrac{1}{3}(2\gamma+1)f. \tag{19}$$

In these asymptotic solutions f is subject to the boundary conditions $f(0)f'(0) = 1$, $f(\eta_e) = 0$ and the integral constraint $\int_0^{\eta_e} f\,\mathrm{d}\eta = 1$ where the location of the leading edge of the current at $\eta = \eta_e$ is determined as part of the solution. In these asymptotic solutions, the region $0 < \eta < \eta_e$ is filled with injected vapour, and beyond this point the vapour pressure is zero. These solutions are exact if the reservoir initially contains no vapour. If the reservoir initially contains vapour, with pressure P_∞, then the similarity solutions are valid either at short times $t \ll (P_\infty/P_o)^{1/\alpha}t^*$ for $\gamma < -\frac{1}{2}$ or at long times $t \gg (P_\infty/P_o)^{1/\alpha}t^*$ for $\gamma > -\frac{1}{2}$. In the short time limit, there is a further restriction that $\gamma > -1$, in order that the mass flux is finite at $t = 0$. The case in which the input pressure is a constant, discussed in §2.1, corresponds to the case $\gamma = -\frac{1}{2}$, for which we showed that the background pressure is non-negligible.

By solving the full nonlinear diffusion equation using an implicit predictor–corrector method (Ames 1977), we have confirmed that the vapour pressure converges to these

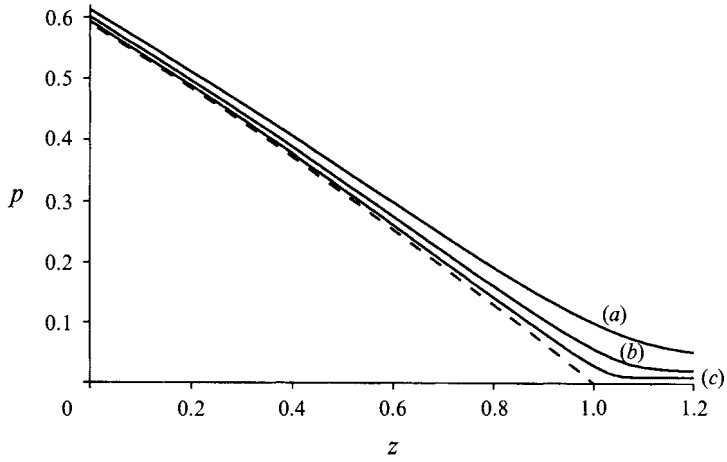

FIGURE 6. Variation of the pressure $(P/P_o)(t^*/t)^{1/3}$ within the reservoir as a function of the dimensionless position $z = (x/L)(t^*/t)^{2/3}$. Curves (solid) calculated from the full numerical model are shown at several times, (*a*) $(P_o/P_\infty)^2(t/t^*) = 0.1$, (*b*) 1 and (*c*) 10 for comparison with the similarity solution (dashed line).

self-similar solutions. For example, figure 6 illustrates the variation of dimensionless pressure as a function of the position across the reservoir at several times $(P_o/P_\infty)^3 t/t^* = 0.1(a)$, $1(b)$ and $10(c)$ as vapour is injected at a constant rate, $\gamma = 0$. The figure shows that for $t > t^*(P_\infty/P_o)^{1/3}$, the full numerical solution (solid lines) for the pressure is very similar to the similarity solution (dashed line). These solutions cease to hold once the pressure reaches the saturation value.

3. Vapour flow in a bounded domain

In a finite domain, the similarity solutions identified in §2 cease to hold once the dynamic pressure signal has traversed the reservoir. We now analyse the longer-term evolution of the pressure within a bounded domain. We focus upon the case in which a constant flux of vapour is added to or removed from the reservoir.

According to (7), the mass flux of vapour D_F which may be transferred across a reservoir of initial background pressure P_∞ and typical length L scales as $D_F \sim kP_\infty(P_s - P_\infty)/(R_g T\mu L)$, where P_s is the saturation pressure coinciding with the reservoir temperature, and P_∞ is the initial reservoir vapour pressure.

After a diffusion time $L^2\phi\mu/(kP_\infty)$, the pressure signal has reached the far boundary and the similarity solutions of §2 do not apply. If the mass flux of vapour across the reservoir D_F far exceeds the imposed flux at the source, Q, so that

$$\frac{kP_\infty(P_s - P_\infty)}{R_g T\mu L} \gg Q, \tag{20}$$

then the vapour pressure in the reservoir becomes nearly uniform. We have solved the full nonlinear diffusion equation (7) for the case of steady injection of vapour at $x = 0$ and with no vapour flow through the far boundary of the reservoir at $x = L$. In figure 7 we show the numerical calculations (solid lines) of the variation with time of the dimensionless pressure, $p = (P - P_\infty)/(P_s - P_\infty)$ at the point of injection of vapour, $x = 0$, and at the far boundary of the reservoir, $x = L$. In this figure, the dimensionless background pressure, $p_\infty = P_\infty/(P_s - P_\infty) = 0.7$, the dimensionless time is defined by

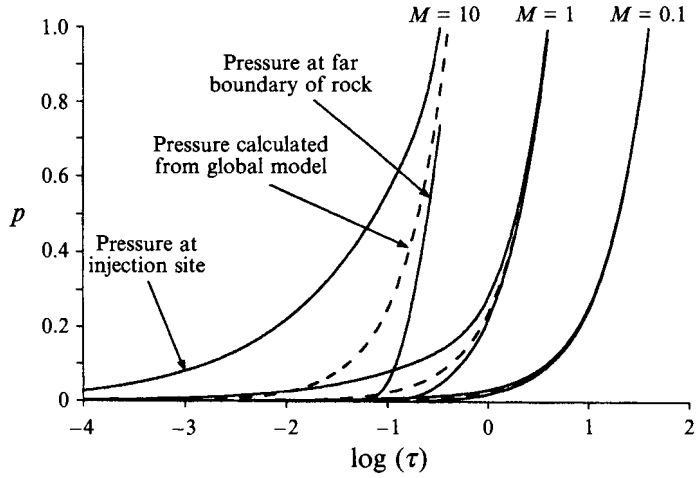

FIGURE 7. Numerical calculations of the variation of the pressure at the input and far end of the reservoir as a function of time for $M = 0.1$, 1 and 10 (solid lines). For comparison, the variations with time of the mean reservoir pressure as calculated from the spatially averaged model are also shown (dashed lines).

$\tau = t(kP_\infty/L^2\mu)$ and curves are shown for dimensionless steady mass fluxes $M = 0.1$, 1 and 10 where $M = QR_g T\mu L/kP_\infty(P_s - P_\infty)$. As more vapour is added to the domain, the pressure increases slowly throughout the reservoir, and becomes increasingly uniform. This is because as the mass of vapour in the rock increases, the average pressure in the rock also rises and therefore the effective coefficient of diffusion $k(P_s - P_\infty)/(\phi\mu)(p + p_\infty)$ increases. Consequently, for a fixed flux of vapour injected into the reservoir, the pressure gradients decrease with time and the vapour pressure becomes more uniform.

For small injection rates, $M \ll 1$, the supply of vapour becomes the rate-limiting process rather than the migration of vapour across the reservoir. Therefore, the pressure becomes approximately uniform long before saturation conditions are approached at the site of injection. The mean dimensionless pressure in the reservoir after vapour has been injected at a dimensionless rate M for a time τ is

$$\bar{p}(\tau) = \int_0^\tau M(\tau')\,\mathrm{d}\tau'. \tag{21}$$

In figure 7 we also show how this spatially averaged pressure $\bar{p}$ varies (dashed lines) with time as vapour is injected at rates $M = 0.1$, 1 and 10. The full numerical solution illustrates that the differences between the injection pressure, the far boundary pressure and the mean reservoir pressure are negligible for slow injection. In this case, $M = 0.1$, the spatially averaged model is very accurate. Furthermore, the averaged model becomes more accurate with time since the effective diffusion coefficient increases with pressure (equation (6)), and so for a given flux, the pressure gradients decrease. For more rapid injection ($M \gg 1$) the pressure gradients remain large, and so the pressure at the injection point continues to exceed the spatially averaged pressure.

For sufficiently slow injection of vapour into a bounded domain, $M \ll 1$, the pressure is approximately uniform so that as more vapour is added, the vapour becomes uniformly compressed. Therefore, the position of the front of new vapour x is approximately given by

$$x/L = \bar{p}/(\bar{p} + p_\infty). \tag{22}$$

As more vapour is added to the reservoir, the vapour pressure increases towards the saturation pressure, at which point the model ceases to hold.

In the case of slow steady extraction of vapour from a reservoir, the dimensionless pressure in the reservoir may be written $p = (P - P_e)/(P_\infty - P_e)$, where P_e is the pressure at the extraction site. If the dimensionless mass flux extracted from the reservoir is $M(\tau)$, then the mean pressure is given by

$$\bar{p}(\tau) = 1 - \int_0^\tau M(\tau')\,\mathrm{d}\tau'. \tag{23}$$

Again, if $M \ll 1$ then the pressure becomes nearly uniform. However, in contrast to vapour injection, the effective coefficient of diffusion in this case decreases as the mass of vapour and reservoir pressure decrease. As a result, the pressure gradients increase with time, and the distribution of vapour pressure becomes less uniform.

4. The injection of water into a bounded rock

Vapour may be generated in geothermal reservoirs through the injection and subsequent vaporization of water (Schroeder *et al.* 1982). Pruess *et al.* (1987) and Woods & Fitzgerald (1993) studied the generation of vapour as water invades an unbounded hot porous layer. They showed that the rate of vaporization of the liquid is controlled by the self-similar motion of the vapour ahead of the interface. However, in §3 we showed that in a bounded domain, for sufficiently slow addition of vapour, the vapour distribution tends to become nearly uniform and the vapour flow ceases to be self-similar. We now apply these results to examine the controls on the generation of vapour through the injection of water into a bounded domain.

If liquid is injected into a vapour-filled porous rock sufficiently rapidly, a sharp interface may develop between the liquid and vapour regions and we focus upon this case in the remainder of this paper (Fitzgerald & Woods 1994). If the temperature of the liquid is lower than the temperature of the hot vapour-filled rock then as the interface advances into the hot rock, it is cooled and the energy released is used to vaporize and heat up a fraction of the liquid. The fraction F of injected water that vaporizes is given by

$$F = 1 - \frac{\phi\rho_w(h_{v\infty} - C_{pw}T_i)}{\phi\rho_w(h_{v\infty} - C_{pw}T_i) + (1-\phi)\rho_r C_{pr}(T_\infty - T_i)}, \tag{24}$$

where h is taken to represent the specific enthalpy, C_p the specific heat capacity, T_i the saturation temperature associated with the pressure at the liquid–vapour interface; subscript r denotes a property of the rock, subscript ∞ a value in the superheated vapour zone, subscript v a property of the vapour and subscript w a property of the liquid water (Woods & Fitzgerald 1993). If we assume that the liquid and vapour are in thermodynamic equilibrium at the liquid–vapour interface then the pressure P_i and temperature T_i are coupled by the Clapeyron relation, which has the approximate form

$$T_i(P) = \chi P_i^{0.23} \tag{25}$$

(Haywood 1972) in the temperature range $150 < T < 240$ °C, where χ is a dimensional constant, with value 6.7 K $(\mathrm{ms^2\,kg^{-1}})^{0.23}$. Equations (24) and (25) may be used to calculate the flux of new vapour produced at the interface and also the rate of advance of the liquid–vapour interface into the vapour region. The new vapour then migrates away from the interface towards the far boundary of the rock with the pressure distribution governed by the nonlinear diffusion equation (6).

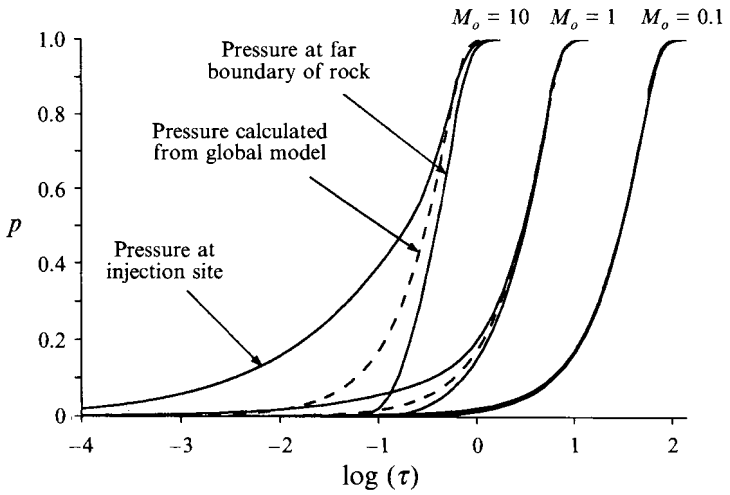

FIGURE 8. Numerical calculations of the variation of the pressure at the vaporizing interface and at the far end of reservoir as a function of time for dimensionless initial vapour fluxes $M_o = 0.1$, 1 and 10 (solid lines). For comparison, the variations with time of the mean reservoir pressure as calculated from the spatially averaged model are also shown (dashed lines).

As in §3, a suitable scale for the vapour flux across the reservoir is $kP_\infty(P_s - P_\infty)/(\mu L R_g T)$ where P_s denotes the saturation pressure of the reservoir associated with the initial temperature of the reservoir (equation (25)). If liquid invades the reservoir at the steady rate Q_w, and a fraction F of this liquid vaporizes, then the dimensionless vapour flux produced at the liquid interface, M, may be written

$$M = \frac{FQ_w R_g T \mu L}{kP_\infty(P_s - P_\infty)} = FM_w, \tag{26}$$

where M_w is the dimensionless liquid flux. As the liquid–vapour interface migrates into the reservoir, F and hence M evolve.

If the liquid flux is small, $M_w \ll 1$, and so $M \ll 1$. Therefore, the reservoir pressure will rapidly become nearly uniform. To test this hypothesis, we have solved numerically the full nonlinear diffusion equation describing the vapour motion ahead of the vaporizing front, (6), coupled with the constraint of zero vapour flux through the far boundary at $x = L$ and the boundary conditions (24) and (25) at the moving liquid–vapour interface. In our calculations, we have set the rate of injection of liquid at $x = 0$, M_w, to be a constant, but note that the liquid–vapour interface advances more slowly than the interstitial speed of the liquid owing to the vaporization of the fraction F of the liquid. In figure 8 we present a full numerical calculation of the dimensionless pressure at the interface and at the far boundary of the domain as a function of the dimensionless time (solid lines), with dimensionless initial vapour flux $M_o = 0.1$, 1 and 10 where subscript o denotes an initial value. Dimensionless pressures are defined as in §3 by $p = (P_i - P_\infty)/(P_s - P_\infty)$. In figure 9 we show how the mass fraction vaporizing, F, varies with time in each of these cases as calculated from the full numerical model (solid lines). In the cases $M_o = 0.1$ and 1, we find that there is an initial adjustment to a nearly uniform pressure throughout the reservoir, which occurs over a dimensionless time $O(1)$ (see figure 8). The initial transient behaviour is similar to the steady injection and subsequent vaporization of liquid in an unbounded domain, as described by Woods & Fitzgerald (1993). This is because in one dimension, vapour is produced at the interface more rapidly than it can migrate ahead of the interface. Therefore, vapour accumulates

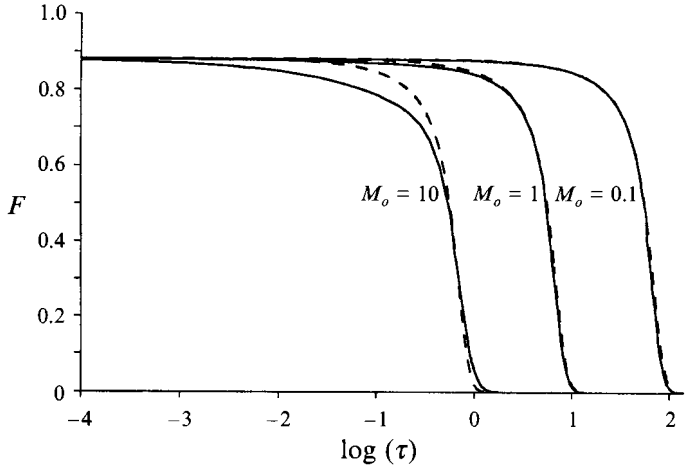

FIGURE 9. Variation of the mass fraction which vaporizes F as a function of time calculated using both the full numerical solution (solid lines) and the averaged model (dashed lines) for steady liquid injection with dimensionless initial vapour fluxes $M_o = 0.1$, 1 and 10.

ahead of the interface resulting in an increase in the interfacial pressure. In turn, this lowers the mass fraction of liquid which vaporizes (Woods & Fitzgerald 1993).

After this transient, owing to the presence of the far boundary of the reservoir, the reservoir vapour pressure becomes nearly uniform and gradually increases towards the saturation value associated with the initial temperature of the reservoir. The mass fraction of the injected liquid which vaporizes therefore decreases towards zero (Figure 9) because less thermal energy is removed from the rock as the vapour pressure increases (cf. Woods & Fitzgerald 1993).

This numerical solution also shows that once $M < 1$, M remains small because as more vapour is added to the reservoir, the dimensionless reservoir pressure $p = (P - P_\infty)/(P_s - P_\infty)$ increases and the mass fraction vaporizing F decreases (cf. Woods & Fitzgerald 1993). In the limit $M \ll 1$, in which the reservoir pressure becomes nearly uniform, we may approximate the interfacial pressure p_i with the average reservoir pressure, $\bar{p}$ say. Using this approximation, F is given approximately from (24) and (25) evaluated at $\bar{p}$; as the liquid continues to invade the rock, that part of the reservoir which contains vapour has approximate extent

$$\frac{L_v}{L} = 1 - \int_0^\tau (1 - F(\bar{p}))\, M_w(\tau')\, \mathrm{d}\tau' \tag{27}$$

and the mean vapour pressure is given by the conservation of mass:

$$\bar{p}(\tau) = \frac{\displaystyle\int_0^\tau F(\bar{p})\, M_w(\tau')\, \mathrm{d}\tau'}{\displaystyle 1 - \int_0^\tau (1 - F(\bar{p}))\, M_w(\tau')\, \mathrm{d}\tau'}, \tag{28}$$

where $M_w(\tau)$ is the dimensionless liquid mass flux. Furthermore, the location of the front of newly injected vapour, $L_n(\tau)$, is given approximately from the conservation of mass and of new vapour as

$$\frac{L_n(\tau)}{L} = \int_0^\tau (1 - F(\bar{p}))\, M_w(\tau')\, \mathrm{d}\tau' + \frac{\bar{p}}{\bar{p} + p_\infty}\left(1 - \int_0^\tau (1 - F(\bar{p}))\, M_w(\tau')\, \mathrm{d}\tau'\right). \tag{29}$$

We have solved this simple uniform-vapour-pressure model of the vaporization of a liquid front advancing into a hot porous reservoir (equations (24), (25), (27), (28)). In figure 8, we compare the predictions of this simple time-dependent model with the full numerical solution of the nonlinear diffusion equation for the vapour flow. The dashed lines in figure 8 show the evolution of the mean reservoir pressure calculated using this uniform-pressure model. The numerical solution shows that in fact when the dimensionless vapour flux $M_o < 1$, the spatially uniform model becomes very accurate. Indeed, the model becomes more accurate with time since, as the mean reservoir pressure increases, the effective diffusion coefficient (equation (7)) increases and so the difference between the interface and far-boundary pressure decreases (cf. §3).

For larger initial fluxes of vapour, $M_o > 1$, the vapour cannot migrate through the reservoir as rapidly as the new vapour is being produced. Thus the far-field pressure and hence average pressure is smaller than that at the interface. As a result, the averaged model predicts a larger rate of production of vapour than the full numerical model. Thus, the averaged model actually predicts that the reservoir becomes vapour saturated at an earlier time than predicted by the full numerical solution.

5. Vapour flow in an open bounded reservoir

In a number of geothermal systems, vapour may enter a reservoir through one boundary while venting from another. We now examine how a steady flow configuration in which there is no net flux of vapour into the reservoir becomes established.

If vapour is injected at one boundary of a reservoir by raising the pressure to P_{in}, while vapour vents from a far boundary maintained at a low pressure, P_{ex}, then high- and low-pressure regions initially diffuse into the reservoir independently. In figure 10, we illustrate this adjustment in the case in which the difference between the injection pressure and the original reservoir pressure equals the difference between the original pressure and the extraction pressure. The average pressure close to the injection site increases and the average pressure close to the extraction site decreases. As a result, the effective diffusion coefficient for the pressure distribution (cf. (6)) increases near the injection site and decreases near the extraction site. This produces a non-uniform pressure gradient which tends to a steady state over a dimensionless time $\tau = \mu\phi L^2/(kP_{ex})$ of order unity. From (6), this steady-state pressure distribution is given as the solution of

$$\frac{\partial}{\partial z}\left((p+p_\infty)\frac{\partial p}{\partial z}\right) = 0 \tag{30}$$

with $p(0) = 1$ and $p(1) = 0$, where the dimensionless pressure $p(z)$ and exit pressure p_∞ are defined as

$$p = \frac{P-P_{ex}}{P_{in}-P_{ex}}, \quad p_\infty = \frac{P_{ex}}{P_{in}-P_{ex}}, \tag{31}$$

and the dimensionless position is given by $z = x/L$. Thus the steady-state pressure profile is

$$p = -p_\infty + (p_\infty^2 + (2p_\infty + 1)(1-z))^{1/2}. \tag{32}$$

When the exit pressure is relatively large compared to the driving pressure $(P_{in}-P_{ex})$, $(p_\infty \gg 1)$, the diffusion coefficient is nearly constant and $p \sim 1-z$. However, when the exit pressure p_∞ is relatively small $(p_\infty \ll 1)$ the effects of the nonlinear diffusion are

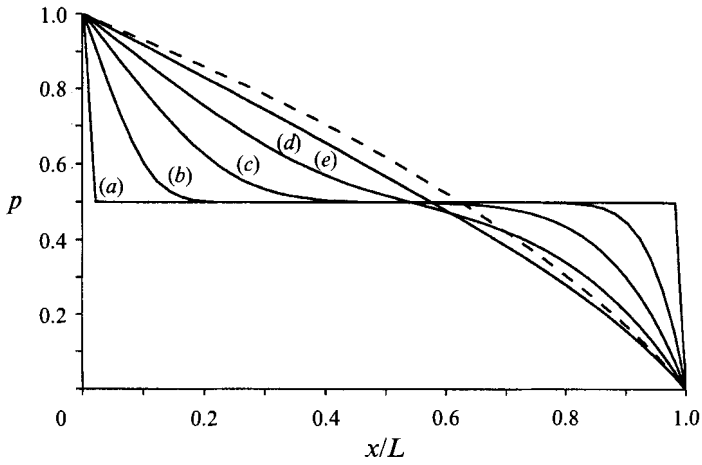

FIGURE 10. Variation of the dimensionless pressure in a porous medium as a function of distance x/L as vapour is simultaneously injected and extracted. Vapour is injected at a pressure $p = 1$ at $x = 0$ and extracted at a pressure $p = 0$ at $x = L$. The solid lines show the pressure profiles at dimensionless times (*a*) 2×10^{-5}, (*b*) 2×10^{-3}, (*c*) 1×10^{-2}, (*d*) 3×10^{-2} and (*e*) 8×10^{-2}. The steady-state profile is shown by the dashed line.

dominant. In the limiting case $p_\infty \to 0$, the vapour pressure has the form $p \sim (1-z)^{1/2}$. These solutions are useful for analysing the slow vaporization of liquid as it invades an open bounded porous region.

6. The injection of liquid into an open bounded reservoir

We now build upon §5 and examine a simple model of the interesting problem in which liquid is steadily injected through one boundary of a geothermal reservoir while vapour, generated at the moving liquid interface, vents from a far boundary at constant pressure, P_{ex}. Following §4, we define the dimensionless vapour flux produced at the moving liquid–vapour interface to be

$$M = \frac{FQ_w R_g T \mu L}{kP_{ex}(P_s - P_{ex})}, \tag{33}$$

where Q_w is the steady liquid flux injected into the reservoir, and F is the mass fraction vaporizing. We also define the dimensionless time $\tau = kP_{ex}\, t/(\mu\phi L^2)$ and the dimensionless pressure $p = (P - P_{ex})/(P_s - P_{ex})$ where P_s is the saturation pressure associated with the initial reservoir temperature. The vapour motion is governed by (6), and as in §4, the mass fraction vaporizing is given by (24) and (25). In figure 11, we present a full numerical solution of the pressure distribution across the reservoir at dimensionless times 0.01, 0.1 and 1, again calculated using an implicit predictor–corrector method (Ames 1977). In this figure, the initial dimensionless vapour flux produced at the advancing liquid interface has value $M_o = 10.0$, and the exit pressure is set equal to the initial reservoir pressure.

During the initial transient, before the pressure signal associated with the new vapour has reached the far boundary of the reservoir, the mass fraction of injected liquid which vaporizes decreases. This initial transient is very similar to that described in §4, and the behaviour may be understood from the results of Woods & Fitzgerald (1993) who considered the case of an unbounded domain. However, once the pressure signal has reached the exit site, a quasi-steady state appears to become established in

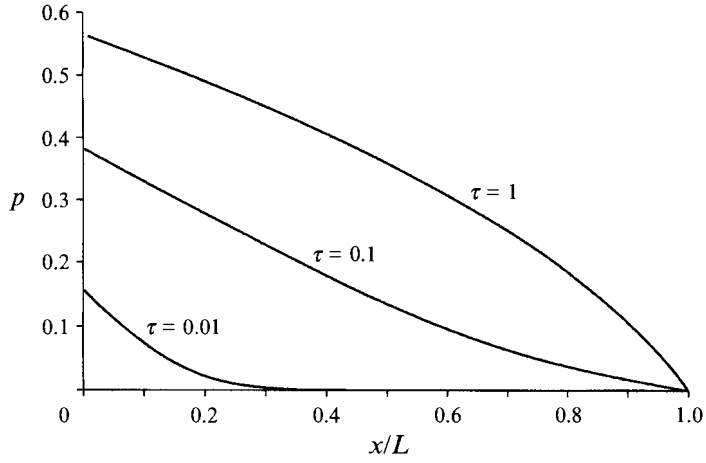

FIGURE 11. Variation of pressure p as a function of distance x/L as vapour is produced from a moving liquid–vapour interface, with liquid injected at a steady rate such that the initial flux of vapour has dimensionless value $M_o = 10$. Pressure distributions are shown at times $\tau = 0.01$, 0.1 and 1.

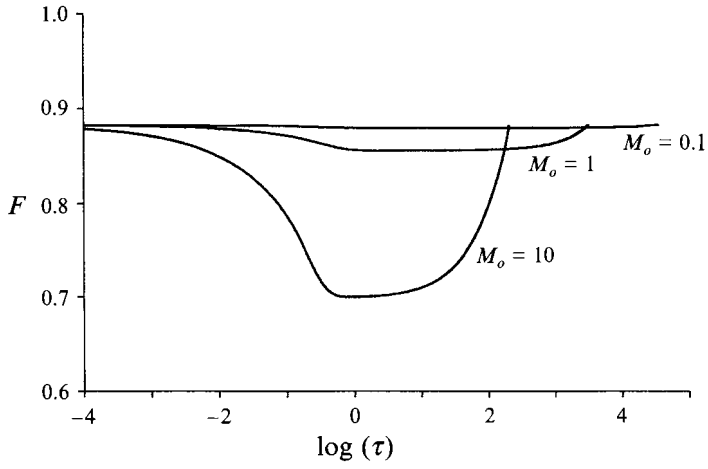

FIGURE 12. Variation of the fraction vaporizing as a function of dimensionless time $\tau = kP_{ex}t/\phi\mu L^2$ as liquid is steadily injected such that the dimensionless initial vapour flux has value $M_o = 0.1$, 1 and 10.

which the vapour flux becomes nearly constant throughout the reservoir. From our numerical calculations, we then observe that as liquid continues to invade the reservoir, the size of the vapour region slowly decreases, the nearly uniform vapour flux slowly increases (figure 12), and the interface pressure slowly decreases (figure 13).

This evolution of the quasi-steady system may be understood as follows. As the size of the vapour-saturated region decreases, the pressure difference between the interface and the exit site which is required to sustain a given vapour flux decreases. However, if the interfacial pressure decreases, the mass fraction which vaporizes tends to increase (Woods & Fitzgerald 1993). Therefore, since the exit pressure P_{ex} is fixed, then, once the quasi-steady state becomes established, the interfacial pressure slowly decreases (figure 13) and the mass fraction which vaporizes slowly increases (figure 12). The process continues until the liquid interface has advanced to the far boundary of the reservoir, and the reservoir has become liquid saturated.

In the limit that the cross-reservoir diffusion time is shorter than the time over which

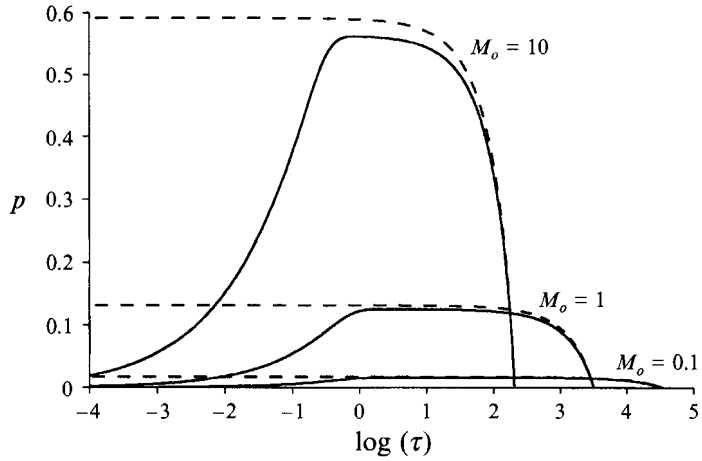

FIGURE 13. Variation of the interfacial pressure as a function of dimensionless time $\tau = kP_{ex}\,t/\phi\mu L^2$, as calculated from the full numerical model (solid lines) and as calculated from the spatially averaged model (dashed lines). In these calculations, liquid is steadily injected such that the dimensionless initial vapour flux has value $M_o = 0.1$, 1, and 10.

the pressure at the liquid–vapour interface changes and also shorter than the time over which the size of the vapour-filled region, L_v, changes,

$$\frac{L_v^2\phi\mu}{kP_o} \ll \frac{P_i}{\mathrm{d}P_i/\mathrm{d}t}, \frac{L_v}{\mathrm{d}L_v/\mathrm{d}t}, \tag{34}$$

we expect that the vapour pressure distribution will approach a quasi-steady solution of the form of (32), corresponding to a spatially uniform vapour flux. In this case, we can develop a quasi-steady time-dependent model of the vapour production and migration in terms of the dimensionless interface position $z_i(\tau)$ and pressure $p_i(\tau)$ which slowly vary with time τ as the liquid invades the reservoir. Following §5, the quasi-steady pressure distribution within the vapour is given by

$$p = -p_\infty + (p_\infty^2 + 2(\tfrac{1}{2}p_i(\tau)^2 + p_\infty p_i(\tau))(1-z_i))^{1/2}, \tag{35}$$

where the constant p_∞ represents the dimensionless exit pressure $p_\infty = P_{ex}/(P_s - P_{ex})$. The interfacial pressure $p_i(\tau)$ may be determined by equating the two dimensionless expressions for the mass flux of vapour at the interface:

$$F(p_i)\,M_w = -p_i(\tau)\left.\frac{\partial p}{\partial z}\right|_{z=z_i}, \tag{36}$$

where M_w is the dimensionless liquid flux, the mass fraction vaporizing $F = F(p_i(\tau))$ is given by (24), the size of the vapour-saturated region at dimensionless time τ is

$$1 - z_i = \int_0^\tau (1 - F(\tau'))\,M_w(\tau')\,\mathrm{d}\tau' \tag{37}$$

and $\partial p/\partial z|_{z=z_i}$ is evaluated using (35).

Equation (34) suggests that this quasi-steady model is valid when $(1/p_i)/\mathrm{d}p_i/(\mathrm{d}z_i) \ll 1$. From (35), we may write $p_i(\tau) = \tilde{p}_i(z_i)$ and so $\mathrm{d}p_i/\mathrm{d}\tau = (\mathrm{d}\tilde{p}_i/\mathrm{d}z_i)/(\mathrm{d}z_i/\mathrm{d}\tau)$. Also, from (37) it follows that the vapour-filled region contracts at a rate $(\mathrm{d}z_i/\mathrm{d}\tau = M_w(1-F)$. Therefore, we expect the model to be valid when

$$\left.\frac{\mathrm{d}\tilde{p}_i}{\mathrm{d}z_i}\right|_{z=z_i} \frac{M_1(1-F)}{p_i} \ll 1. \tag{38}$$

Typically, this is the case if the flux of liquid $M_w \ll 1.0$. Condition (38) also has a weak dependence upon F, which typically lies in the range $0.1 < F < 0.8$ and which varies with the superheat of the reservoir (Woods & Fitzgerald 1993).

In order to test the validity of this quasi-steady model, we now compare a number of numerical solutions of the full model with the predictions of this simplified uniform flux model. In figure 13 we show how the interfacial pressure $p_i(\tau)$ varies with time for three values of the initial dimensionless vapour flux produced at the advancing liquid interface, $M_o = 0.1$, 1.0 and 10.0. The solid lines denote the solution of a numerical model including the full time-dependent nonlinear pressure diffusion equation (7), while the dashed lines are the predictions of the quasi-steady uniform-flux model described above. With $M_o = 0.1$, the quasi-steady model rapidly converges to the full numerical solution, once the pressure signal has migrated across the reservoir. This takes a dimensionless time of order unity. At longer times, the quasi-steady model is in very good agreement with the numerical solution. However, as expected from (38), for larger fluxes of vapour (e.g. $M_o = 1.0$, 10.0), the process remains transient since the rate of vapour production increases with time and so vapour is supplied to the moving liquid interface more rapidly than it can spread across the reservoir.

7. Conclusions

We have presented a series of models to describe the motion of vapour through a hot porous rock. First, we showed that, in an unbounded rock, the vapour migrates in a self-similar fashion from an injection site. Our similarity solutions also identified that the newly input vapour actually lags behind the pressure signal as a result of the compression of the original vapour in the reservoir. This is of import for monitoring geothermal systems, since at an observation well, a dynamic pressure signal will be observed before any geochemical changes resulting from differences between host and input fluids. These similarity solutions are complementary to those presented by Woods & Fitzgerald (1993) to describe the motion of a vaporizing liquid front as it invades an unbounded reservoir.

Next we considered the injection of vapour into a bounded reservoir. We showed that in the limit that the injected vapour flux is small compared to the maximum flux of vapour which may migrate across the reservoir, the vapour pressure becomes approximately uniform. As vapour continues to invade the reservoir, the reservoir pressure then gradually increases towards saturation conditions. Also, since the vapour originally in place has to be compressed as new vapour enters the rock, new vapour does not actually reach the far boundary of the reservoir before the reservoir becomes saturated. Using these results, we have developed a simple time-dependent model of the vaporization of water slowly invading a hot bounded porous rock, based upon the assumption of a uniform vapour pressure, combined with the Stefan condition at the moving liquid–vapour interface. In accord with a full numerical calculation which accounts for the spatial distribution of the vapour, the approximate model shows that as the reservoir pressure increases, the rate of vaporization decreases, until the reservoir becomes vapour saturated. The steady decrease in the rate of vaporization is a result of the increase in interfacial temperature which accompanies the increase in interfacial pressure; increasing the interfacial temperature reduces the thermal energy released by the hot rock as it is invaded by the liquid.

Finally, we considered the case in which vapour is simultaneously injected into and extracted from a bounded rock. We showed that over the cross-reservoir diffusion time the mass flux of vapour becomes spatially uniform. We then developed this result to

show that if water is slowly injected into a bounded rock while vapour is simultaneously extracted from the far boundary, the system rapidly evolves to a quasi-steady state in which the vapour flux is spatially uniform. As the liquid continues invading the domain, this quasi-steady state gradually evolves. The mass fraction of liquid which vaporizes gradually increases because as the size of the vapour-filled region of the reservoir decreases, the interfacial pressure also decreases. This causes an increase in the mass fraction which vaporizes since more heat can be released from the host rock as the interfacial pressure and hence temperature decrease. In an Appendix, we extend the analysis to consider the production and migration of vapour in two-dimensional bounded reservoirs. Again, the spatially averaged model works well for a wide range of operating conditions.

The models of vapour production and migration which we have developed in this paper are highly idealized, in order to focus upon the underlying physical controls. In geothermal reservoirs, the geometry of injection and extraction may be very complex, the reservoir may be spatially inhomogeneous and non-isothermal. Furthermore, if the mass fraction which vaporizes is sufficiently large, then the liquid vapour interface may become unstable (Fitzgerald & Woods 1994). However, noting the limitations, our simple models provide some important constraints on liquid and vapour flows in those geothermal reservoirs which may be described as porous media. For example, the upper depleted zones of the Larderello reservoir have typical properties $P_s \sim 30$ bar, $P_\infty \sim 10$ bar, $k \sim 10^{-14}$ m^2 and vapour viscosity $\mu \sim 10^{-5}$ kg m^{-2} s^{-1} (Pruess *et al.* 1987). Therefore, for two-dimensional recharge (see the Appendix), the maximum cross-reservoir flux of vapour, which scales as

$$Q_a \sim \frac{kP_\infty(P_s - P_\infty)}{R_g T \mu} \text{kg ms}^{-1}, \tag{39}$$

is of order 10^{-1}–10^{-2} kg ms^{-1}. Hence, the models of spatially uniform vapour or vapour flux described herein may be applied to situations in which the applied mass flux per unit depth $Q < 10^{-2}$ kg ms^{-1}. For higher injection rates, the system evolves transiently, and a full numerical solution of the nonlinear diffusion equation for vapour flow is required. A simple application of the quasi-steady model describing the inflow of water and outflow of vapour (Appendix), suggests that a depleted zone of the Larderello geothermal reservoir of temperature 240 °C, radius 3 km, porosity 0.05, initial pressure 10 bar and permeability 10^{-14} m^2 may be used to produce vapour for a period of about 30 years if liquid is injected at a rate of 10^{-2} kg ms^{-1}. After this time the liquid front will have reached the far boundary of the zone. In contrast, zones which are of radius 1 km may be used for about 3 years while those of radial extent 10 km may be used for approximately 300 years.

M. G. Worster and J. R. Lister gave some useful comments on this work. This research was supported by NERC and A.W.W. acknowledges support from the GFD programme at WHOI.

Appendix

Many geothermal systems involve more complex flow geometries than the model one-dimensional flows described in this paper. In particular, flows with cylindrical geometry may be common, and so in this Appendix we extend the methods presented in this paper to describe the production and migration of vapour in a bounded cylindrical domain.

The vapour flux across a cylindrical surface of given radius, in a two-dimensional geometry, scales as

$$Q \sim kP_\infty(P_s - P_\infty)/(\mu R_g T) \tag{A 1}$$

per unit depth. If the rate of addition of water to the system is Q_w per unit depth, then the dimensionless vapour flux at the advancing liquid–vapour interface may be written

$$M = FM_w = FQ_w/Q, \tag{A 2}$$

where F is the mass fraction of liquid which vaporizes. Note that in contrast to one-dimensional injection, for two-dimensional flow the parameter M is independent of the spatial scale. If $M < 1$, then vapour may migrate across the reservoir more rapidly than it is supplied through vaporization of liquid. In this limit, we expect two different vaporization regimes which depend upon whether the pressure signal associated with the new vapour has reached the far boundary of the reservoir (cf. §3).

Woods & Fitzgerald (1993) presented a family of similarity solutions which modelled the production of vapour as water spreads radially from a line source into an unbounded hot permeable rock. For a constant rate of injection, they showed that a constant fraction vaporizes and, therefore, that the position of the interface increases at a rate $r = \lambda(\alpha t)^{1/2}$ where λ is a constant and α is the effective diffusion coefficient $\alpha = k(P_s - P_\infty)/(\phi\mu)$. The vapour pressure ahead of this front was shown to be a function of the similarity variable $\eta = r/(\alpha t)^{1/2}$ and the vapour pressure satisfied the similarity equation (cf. (6))

$$-\frac{\mathrm{d}p}{\mathrm{d}\eta}\frac{\eta^2}{2} = \frac{\mathrm{d}}{\mathrm{d}\eta}\left((p+p_\infty)\eta\frac{\mathrm{d}p}{\mathrm{d}\eta}\right). \tag{A 3}$$

For injection from a cylindrical well of finite radius, r_i, the similarity solution is attained after an initial transient which lasts for a time of the order of $t_s = r_i^2/\alpha$. In a bounded domain this similarity solution describes the vaporization until the pressure signal associated with the vapour reaches the far boundary of the reservoir. This occurs after a time of the order of $t_b = L^2\phi\mu/(k(P_s - P_\infty))$, where L is the spatial scale of the reservoir. Once the pressure signal reaches the far boundary, the vaporization process diverges from the similarity solutions.

In the case of a closed bounded region, the vapour pressure becomes approximately uniform (cf. §5) and we may develop a simplified model by assuming that the vapour pressure is uniform. If the region occupied by the vapour has volume $\pi(l^2 - r_f^2)$ per unit depth, then the average pressure increase associated with the production of new vapour is

$$\bar{p} = \int \frac{2r(1 - F(\bar{p}))\, M_w(\tau)\, \mathrm{d}\tau}{l^2 - r_f^2}. \tag{A 4}$$

where l is the spatial scale of the reservoir and r_f denotes the position of the liquid–vapour interface. The fraction which vaporizes may be found from (24) and (25). Since the mean vapour pressure increases with time, the rate of vaporization progressively decreases. As a result, the rate of advance of the liquid front steadily increases relative to the self-similar solution. These effects are illustrated in figure 14(a, b), in which predictions of the full numerical solution (solid line) are compared with the similarity solution (dotted line) and the predictions of the spatially averaged model (dashed lines). For the model run, in these figures, the dimensionless time $\tau = t/t_b$, $r_i/L = 0.04$, $t_s/t_b = 0.002$, $M_w = 1.32$ and $F_s M_w = 1$, where F_s is the fraction vaporizing as predicted from the similarity solution. The full numerical solution converges rapidly to the similarity solution when $\tau \sim O(0.01)$. However, once the

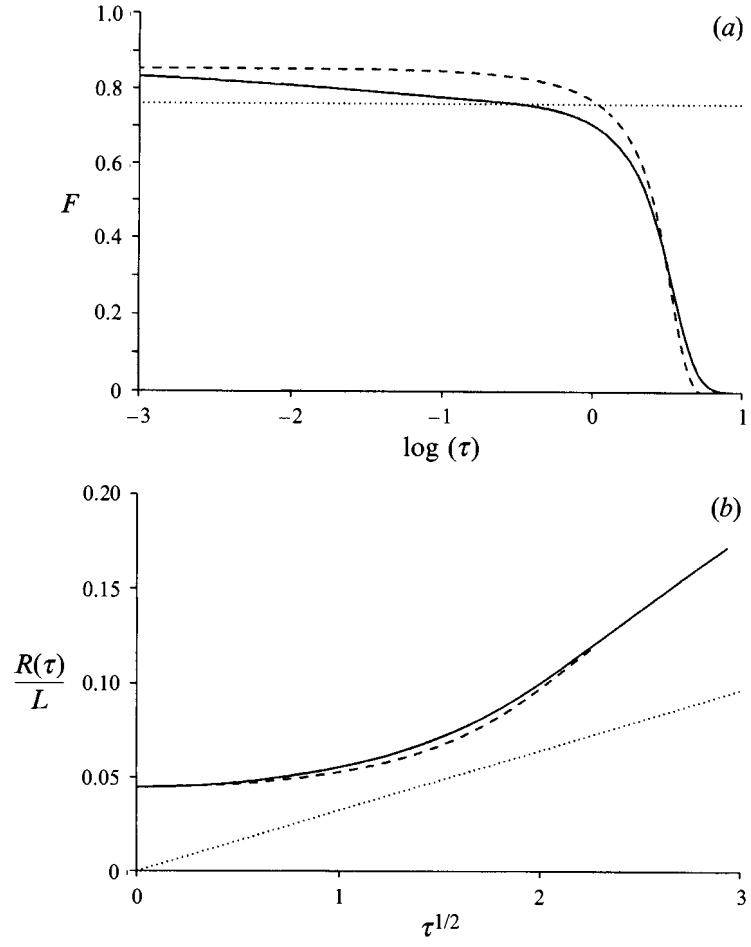

FIGURE 14. Variation of (*a*) the mass fraction vaporizing and (*b*) the position of the liquid–vapour interface as a function of time τ for injection of liquid into a bounded and closed cylindrical reservoir in which $\alpha = 0.06$, $r_i/L = 0.04$, $t_s/t_b = 0.002$, $M_w = 1.32$ and $F_s M_w = 1$ where F_s is the mass fraction vaporizing as determined from the similarity solution. Solid lines represent the full numerical solution in the case that the initial pressure distribution is uniform, dotted lines are the similarity solution for an unbounded domain (Woods & Fitzgerald 1993) and dashed lines are the predictions of the model using a spatially averaged pressure.

pressure signal has reached the far boundary, at time $\tau \sim O(1)$, the full solution becomes nearly indistinguishable from the spatially averaged model, up to the time at which the vapour becomes saturated (cf. §5). Further calculations show that, as expected, for $M > 1.0$, the uniform-pressure model is less accurate, particularly in respect of the prediction of the mass fraction vaporized.

In the case of an open boundary, the mean vapour flux across any cylindrical surface, centred on the injection well, becomes nearly independent of radius once the pressure signal associated with the vapour flux has reached the far boundary of the reservoir. The pressure distribution across the reservoir is then given by the approximate relation (cf. §6)

$$p = -p_i + \left(p_\infty^2 + 2(\tfrac{1}{2}p_i^2 + p_i p_\infty)\log\left(\frac{A+\hat{x}}{A+1}\right)\Big/\log\left(\frac{A}{A+1}\right)\right), \tag{A 5}$$

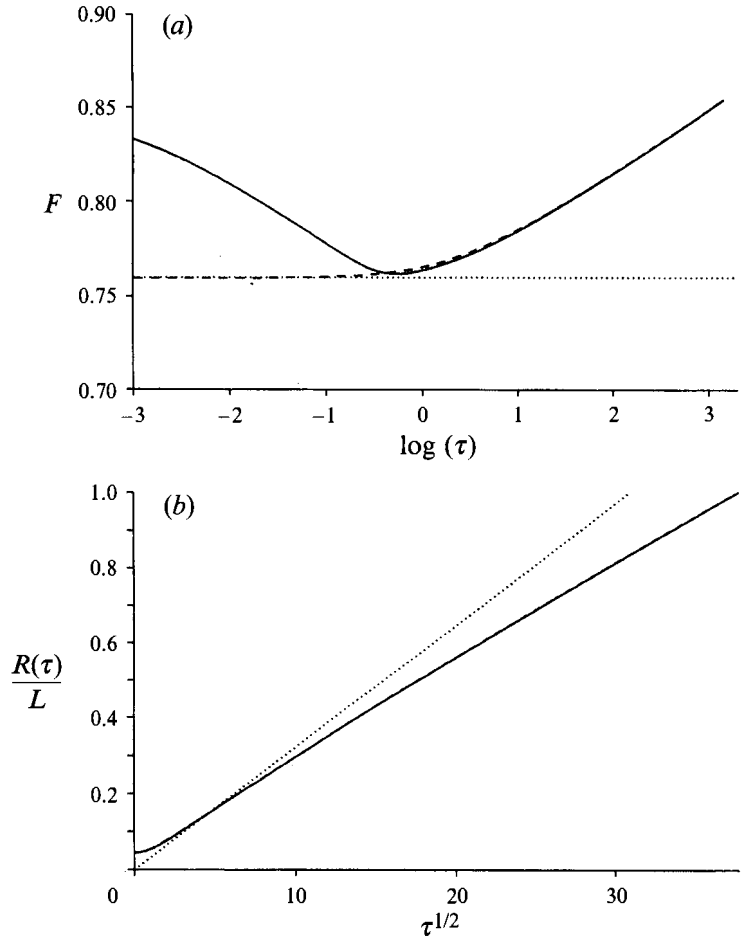

FIGURE 15. As figure 14 but for a bounded and open cylindrical reservoir.

where $A = r_i/L$ and $\hat{x} = (r-r_i)/L$. As a consequence, the interfacial pressure begins to fall and the mass fraction of the liquid which vaporizes increases. Thus, the rate of vapour production increases and the interface advances more slowly then predicted by the similarity solution (cf. §6). The full numerical solution shown in figure 15 shows that the similarity solution applies for times $t_s < t < t_b$, while subsequently the uniform-flux model, (A 5), gives a good representation of the process. Further numerical calculations suggest that the agreement improves as M decreases, and that again it is particularly good for $M \leqslant 1$.

Similar models may be developed for the three-dimensional migration of vapour produced from a point source.

REFERENCES

AMES, W. F. 1977 *Numerical Methods for Partial Differential Equations*. Nelson.

AXELSSON, G. & BODVARSSON, G. 1987 Analysis of production data from fractured liquid dominated geothermal reservoirs in Iceland. *Trans. Geotherm. Res. Counc.* **11**, 573–580.

BEAR, J. 1972 *Dynamics of Fluids in Porous Media*. Dover.

BODVARSSON, G. 1972 Thermal problems in the siting of reinjection wells. *Geothermics* **1**, 63–66.

CATHLES, L. M. 1977 An analysis of the cooling of intrusives by ground-water convection which includes boiling. *Econ. Geol.* **72**, 804–826.

CLINE, J. S., BODNAR, R. J. & RIMSTIDT, J. D. 1992 Numerical simulation of fluid flow and silica transport and deposition in boiling hydrothermal solutions: application to epithermal gold deposits. *J. Geophys. Res.* **97** (B6), 9085–9103.

D'AMORE, F., CELATI, R., FERRARA, G. C. & PANICHI, C. 1977 Secondary changes in the chemical and isotopic composition of the geothermal fluids in Larderello field. *Geothermics* **5**, 153–163.

DONALDSON, I. G. 1962 Temperature gradients in the upper layers of the earth's crust due to convective water flows. *J. Geophys. Res.* **67**, 3449–3459.

DONALDSON, I. G. 1968 The flow of steam water mixtures through permeable beds: a simple simulation of a natural undisturbed hydrothermal region. *N.Z. J. Sci.* **11**, 3–23.

DUCHI, V., MINISSALE, A. & MANGANELLI, M. 1992 Chemical composition of natural deep and shallow hydrothermal fluids in the Larderello geothermal field. *J. Volcanol. Geotherm. Res.* **49**, 313–328.

DULLEN, F. A. L. 1992 *Porous Media Fluid Transport and Pore Structure.* Academic.

DUNN, J. C. & HARDEE, H. C. 1981 Superconvecting geothermal zones. *J. Volcanol. Geotherm. Res.* **11**, 189–201.

ELDER, J. 1981 *Geothermal Systems.* Academic.

ENEDY, K. L. 1989 The role of decline curve analysis at The Geysers. *Trans. Geotherm. Res. Counc.* **13**, 383–391.

FITZGERALD, S. D. & WOODS, A. W. 1994 The instability of a vaporisation front in hot porous rock. *Nature* **367**, 450–453.

FRADKIN, L. J., SOREY, M. J. & MCNABB, A. 1981 On identification and validation of some geothermal models. *Water Resources Res.* **17**, 929–936.

GOYAL, K. P. & BOX, W. T. 1990 Reservoir response to production: Castle Rock Springs Area, East Geysers, California, USA. *Proc. Stanford Geotherm. Workshop* **15**, 103–112.

GRANT, M. A., DONALDSON, I. G. & BIXLEY P. F. 1982 *Geothermal Reservoir Engineering.* Academic.

HAYWOOD, R. W. 1972 *Thermodynamic Tables in SI (Metric) Units.* Cambridge University Press.

HURST, A. W. & DIBBLE, R. R. 1981 Bathymetry, heat output and convection in Ruapehu crater lake, New Zealand. *J. Volcan. Geotherm. Res.* **9**, 215–236.

KERR, R. A. 1991 Geothermal tragedy of the commons. *Science* **253**, 134–135.

MARTINI, M., GIANNINI, L., BUCCIANTI, A., PRATI, F., CELLINI LEGITTIMO, P., IOZZELLI, P. & CAPACCIONO, B. 1991 1980–1990: Ten years of geochemical investigation at Phlegrean Fields (Italy). *J. Volcanol. Geotherm. Res.* **48**, 161–171.

NORTON, D. & KNIGHT, J. 1977 Transport phenomena in hydrothermal systems: cooling plutons. *Am. J. Sci.* **277**, 937–981.

PARMENTIER, E. M. & SCHEDL, A. 1981 Thermal aureoles of igneous intrusions: some possible indications of hydrothermal convective cooling. *J. Geol.* **89**, 1–22.

PHILLIPS, O. M. 1991 *Flow and Reactions in Permeable Rocks.* Cambridge University Press.

PRUESS, K., CALORE, C., CELATI, R. & WU, Y. S. 1987 An analytical solution for heat transfer at a boiling front moving through a porous medium. *Intl J. Heat Mass Transfer* **30**, 2595–2602.

RUBIN, A. & SCHWEITZER, S. 1972 Heat transfer in porous media with phase change. *Intl J. Heat Mass Transfer* **15**, 43–60.

SCHROEDER, R. C., O'SULLIVAN, M. J., PRUESS, K., CELATI, R. & RUFFILLI, C. 1982 Reinjection studies of vapour-dominated systems. *Geothermics* **11**, 93–119.

TRUESDELL, A. H. & WHITE, D. E. 1973 Production of superheated steam from vapour-dominated geothermal reservoirs. *Geothermics* **2**, 154–173.

WOHLETZ, K. & HEIKEN, G. 1992 *Volcanology and Geothermal Energy.* California.

WOODS, A. W. & FITZGERALD, S. D. 1993 The vaporization of a liquid front moving through a hot porous rock. *J. Fluid Mech.* **251**, 563–579.